JACS
JOURNAL OF THE AMERICAN CHEMICAL SOCIETY

Subscriber access provided by ISTANBUL TEKNIK UNIV

Article

Antibiotic Deactivation by a Dizinc β-Lactamase: Mechanistic Insights from QM/MM and DFT Studies

Dingguo Xu, Hua Guo, and Qiang Cui

J. Am. Chem. Soc., **2007**, 129 (35), 10814-10822• DOI: 10.1021/ja072532m • Publication Date (Web): 11 August 2007

Downloaded from http://pubs.acs.org on February 15, 2009

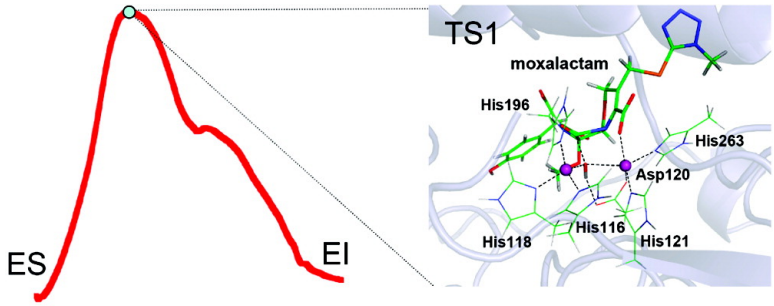

More About This Article

Additional resources and features associated with this article are available within the HTML version:

- Supporting Information
- Links to the 1 articles that cite this article, as of the time of this article download
- Access to high resolution figures
- Links to articles and content related to this article
- Copyright permission to reproduce figures and/or text from this article

View the Full Text HTML

ACS Publications
High quality. High impact.

Journal of the American Chemical Society is published by the American Chemical Society. 1155 Sixteenth Street N.W., Washington, DC 20036

J|A|C|S
ARTICLES
Published on Web 08/11/2007

Antibiotic Deactivation by a Dizinc β-Lactamase: Mechanistic Insights from QM/MM and DFT Studies

Dingguo Xu,[†] Hua Guo,*[,†] and Qiang Cui[‡]

Contribution from the Department of Chemistry and Chemical Biology, University of New Mexico, Albuquerque, New Mexico 87131, Department of Chemistry and Theoretical Chemistry Institute, University of Wisconsin, Madison, Wisconsin, 53706

Received April 11, 2007; E-mail: hguo@unm.edu

Abstract: Hybrid quantum mechanical/molecular mechanical (QM/MM) methods and density functional theory (DFT) were used to investigate the initial ring-opening step in the hydrolysis of moxalactam catalyzed by the dizinc L1 β-lactamase from *Stenotrophomonas maltophilia*. Anchored at the enzyme active site via direct metal binding as suggested by a recent X-ray structure of an enzyme−product complex (Spencer, J.; et al. *J. Am. Chem. Soc.* **2005**, *127*, 14439), the substrate is well aligned with the nucleophilic hydroxide that bridges the two zinc ions. Both QM/MM and DFT results indicate that the addition of the hydroxide nucleophile to the carbonyl carbon in the substrate lactam ring leads to a metastable intermediate via a dominant nucleophilic addition barrier. The potential of mean force obtained by SCC-DFTB/MM simulations and corrected by DFT/MM calculations yields a reaction free energy barrier of 23.5 kcal/mol, in reasonable agreement with the experimental value of 18.5 kcal/mol derived from k_{cat} of 0.15 s^{-1}. It is further shown that zinc-bound Asp120 plays an important role in aligning the nucleophile, but accepts the hydroxide proton only after the nucleophilic addition. The two zinc ions are found to participate intimately in the catalysis, consistent with the proposed mechanism. In particular, the Zn_1 ion is likely to serve as an "oxyanion hole" in stabilizing the carbonyl oxygen, while the Zn_2 ion acts as an electrophilic catalyst to stabilize the anionic nitrogen leaving group.

1. Introduction

The rapidly increasing prevalence of penicillin-resistant bacterial strains poses a great challenge to the future treatment of infectious diseases.[1,2] The most common mode of drug resistance in many pathogenic bacteria is conferred by β-lactamases. These are bacterial enzymes that deactivate penicillin and its analogues by catalyzing the hydrolytic cleavage of the amide (C−N) bond in the functionally conserved lactam ring.[3] Historically, β-lactamases have been divided into four classes, in which Class A, C, and D enzymes utilize an active-site serine in covalent catalysis, while those in Class B require one or two Zn(II) ions to activate the water nucleophile. The catalytic mechanism of the serine-based β-lactamases is well-known, and effective inhibitors have been developed.[4] On the other hand, neither substrate binding nor catalysis of the less known Class B metallo-β-lactamases (MβLs) is well understood,[5,6] a fact that is reflected by the absence of clinically useful inhibitors for these enzymes. Although the occurrence of MβLs is still low, they pose a potentially devastating threat because of their broad substrate profiles, which often encompass nearly all β-lactam antibiotic compounds.[5] The threat looms larger every day because of rapid proliferation of MβLs in opportunistic pathogenic bacteria such as *Pseudomonas aeruginosa* and *Stenotrophomonas maltophilia*.[7] The acquisition of the MβL genes by major pathogens is only a matter of time. The outlook is very troubling without effective inhibitors of MβLs, which in turn require detailed knowledge on the binding and catalysis.

MβLs are further divided into three subclasses.[5,8] Except for B2 enzymes, all MβLs (subclasses B1 and B3) typically have two zinc cofactors. The MβL we are concerned with in this work, namely L1 from *S. maltophilia*, is a representative member of the B3 subclass and has been investigated both structurally[9,10] and kinetically.[11−19] This enzyme is an important source of drug resistance and has a very broad substrate profile,

[†] University of New Mexico.
[‡] University of Wisconsin.

(1) Neu, H. C. *Science* **1992**, *257*, 1064.
(2) Walsh, C. *Nature* **2000**, *406*, 775.
(3) Knowles, J. R. *Acc. Chem. Res.* **1985**, *18*, 97.
(4) Fisher, J. F.; Meroueh, S. O.; Mobashery, S. *Chem. Rev.* **2005**, *105*, 395.
(5) Bush, K. *Clin. Infect. Dis.* **1998**, *27*, S48.
(6) Crowder, M. W.; Spencer, J.; Vila, A. J. *Acc. Chem. Res.* **2006**, *45*, 13650.
(7) Walsh, T. R.; Toleman, M. A.; Poirel, L.; Nordmann, P. *Clin. Microbiol. Rev.* **2005**, *18*, 306.
(8) Galleni, M.; Lamotte-Brasseur, J.; Rossolini, G. M.; Spencer, J.; Dideberg, O.; Frere, J.-M. *Antimicrob. Agents Chemother.* **2001**, *45*, 660.
(9) Ullah, J. H.; Walsh, T. R.; Taylor, I. A.; Emery, D. C.; Verma, C. S.; Gamblin, S. J.; Spencer, J. *J. Mol. Biol.* **1998**, *284*, 125.
(10) Spencer, J.; Read, J.; Sessions, R. B.; Howell, S.; Blackburn, G. M.; Gamblin, S. J. *J. Am. Chem. Soc.* **2005**, *127*, 14439.
(11) Yang, K.-W.; Crowder, M. W. *Arch. Biochem. Biophys.* **1999**, *368*, 1.
(12) McManus-Munoz, S.; Crowder, M. W. *Biochemistry* **1999**, *38*, 1547.
(13) Spencer, J.; Clarke, A. R.; Walsh, T. R. *J. Biol. Chem.* **2001**, *276*, 33638.
(14) Carenbauer, A. L.; Garrity, J. D.; Periyannan, G.; Yates, R. B.; Crowder, M. W. *BMC Biochem.* **2002**, *3*, 4.
(15) Simm, A. M.; Higgins, C. S.; Carenbauer, A. L.; Crowder, M. W.; Bateson, J.; Bennett, P. M.; Clarke, A. R.; Halford, S. E.; Walsh, T. R. *J. Biol. Chem.* **2002**, *277*, 24744.
(16) Garrity, J. D.; Carenbauer, A. L.; Herron, L. R.; Crowder, M. W. *J. Biol. Chem.* **2004**, *279*, 920.
(17) Garrity, J. D.; Pauff, J. M.; Crowder, M. W. *J. Biol. Chem.* **2004**, *279*, 39663.
(18) Garrity, J. D.; Bennett, B.; Crowder, M. W. *Biochemistry* **2005**, *44*, 1078.

 10.1021/ja072532m CCC: $37.00 **© 2007 American Chemical Society**

Scheme 1. Definition of Atoms and Proposed Mechanism for the Initial Ring-Opening Step in Moxalactam Hydrolysis Catalyzed by L1

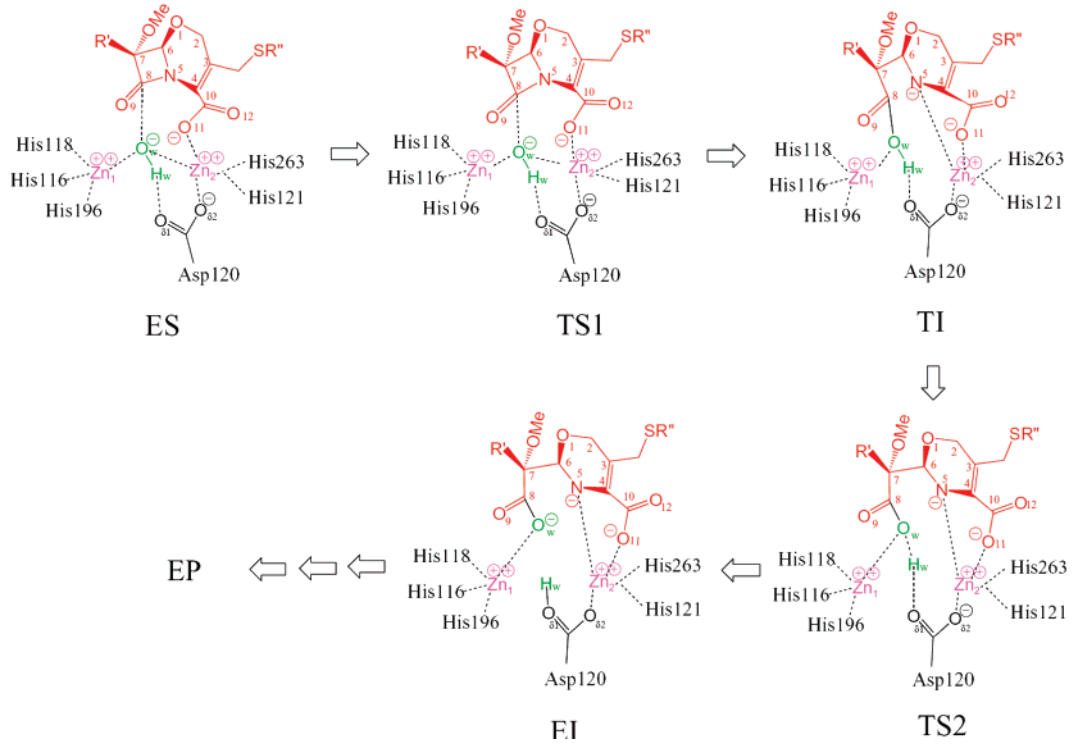

hydrolyzing nearly all β-lactam compounds.[20] An important breakthrough was made recently concerning the enzyme recognition of β-lactam antibiotics, in which Spencer et al.[10] determined the first high-resolution structure of a dizinc MβL (L1) complexed with a substrate analogue (hydrolyzed moxalactam). Such a feat has only been achieved for two MβLs so far, the other being the monozinc CphA enzyme from *Aeromonas hydrophila*.[21] This new development allowed us to recover in an unambiguous fashion the structure of the enzyme−substrate complex using a computational approach,[22] which laid the ground work for the understanding of the chemical steps reported here.

The lactam ring-opening step catalyzed by MβLs is believed to be initiated by the attack on the lactam carbonyl carbon (C_8) by an active-site water/hydroxide (see Scheme 1 for atom definitions).[6,23] In dizinc MβLs, the nucleophilic hydroxide is in a bridging position between two zinc ions, each coordinated by three protein ligands.[9,10] In L1, the three ligands in the so-called Zn_1 site are His116, His118, and His196, whereas those in the Zn_2 position are His121, His263, and Asp120. The addition of the OH^- moiety to C_8 leads to cleavage of the lactam C−N bond, possibly via a tetrahedral intermediate (TI). The resulting anionic nitrogen leaving group is believed to be stabilized by the Zn_2 ion in a kinetically competent intermediate state before its final protonation.[12,13,18,24−26]

Despite the accumulation of structural and kinetic data, the details of the enzymatic reaction are still lacking. Chief among mechanistic uncertainties are the roles of the metal cofactors and of the highly conserved metal-bound Asp120, the existence of a TI and its stability, and the proton-transfer pathways. Some issues concerning MβL binding and catalysis have been addressed theoretically by several groups,[22,27−40] but few have examined the chemical steps with the explicit inclusion of the protein environment.[41−43] This is largely due to difficulties associated with a quantum mechanical characterization of the metal-containing active site. In this work, we present a thorough quantum mechanical/molecular mechanical (QM/MM) study of the initial catalytic step of a dizinc MβL, specifically, the ring-opening of moxalactam by L1 from *S. maltophilia*, which is thought to limit the catalyzed reaction for most β-lactam antibiotics.[13] The QM region was treated by the self-consistent charge-density functional tight binding (SCC-DFTB) method,[44,45]

(19) Costello, A.; Periyannan, G.; Yang, K.-W.; Crowder, M. W.; Tierney, D. L. *J. Biol. Inorg. Chem.* **2006**, *11*, 351.
(20) Crowder, M. W.; Walsh, T. R.; Banovic, L.; Pettit, M.; Spencer, J. *Antimicrob. Agents Chemother.* **1998**, *42*, 921.
(21) Garau, G.; Bebrone, C.; Anne, C.; Galleni, M.; Frere, J.-M.; Dideberg, O. *J. Mol. Biol.* **2005**, *345*, 785.
(22) Xu, D.; Guo, H.; Cui, Q. *J. Phys. Chem. A* **2007**, *111*, 5630.
(23) Wang, Z.; Fast, W.; Valentine, A. M.; Benkovic, S. J. *Curr. Opin. Chem. Biol.* **1999**, *3*, 614.
(24) Wang, Z.; Fast, W.; Benkovic, S. J. *J. Am. Chem. Soc.* **1998**, *120*, 10788.
(25) Wang, Z.; Fast, W.; Benkovic, S. J. *Biochemistry* **1999**, *38*, 10013.
(26) Kaminskaia, N. V.; Spingler, B.; Lippard, S. J. *J. Am. Chem. Soc.* **2001**, *123*, 6555.
(27) Diaz, N.; Suarez, D.; Merz, K. M. Jr. *J. Am. Chem. Soc.* **2000**, *122*, 4197.
(28) Salsbury, J. F. R.; Crowley, M. F.; Brooks, C. L., III. *Proteins* **2001**, *44*, 448.
(29) Suarez, D.; Diaz, N.; Merz, K. M., Jr. *J. Comput. Chem.* **2002**, *23*, 1587.
(30) Suarez, D.; Brothers, E. N.; Merz, K. M., Jr. *Biochemistry* **2002**, *41*, 6615.
(31) Gu, W.; Zhu, J.; Liu, H. *J. Theor. Comp. Chem.* **2002**, *1*, 62.
(32) Dal Peraro, M.; Vila, A. J.; Carloni, P. *Inorg. Chem.* **2003**, *42*, 4245.
(33) Krauss, M.; Gresh, N.; Antony, J. *J. Phys. Chem. B* **2003**, *107*, 1215.
(34) Olsen, L.; Antony, J.; Ryde, U.; Adolph, H.-W.; Hemmingsen, L. *J. Phys. Chem. B* **2003**, *107*, 2366.
(35) Olsen, L.; Rasmussen, T.; Hemmingsen, L.; Ryde, U. *J. Phys. Chem. B* **2004**, *108*, 17639.
(36) Dal Peraro, M.; Vila, A. J.; Carloni, P. *Proteins* **2004**, *54*, 412.
(37) Park, H.; Merz, K. M., Jr. *J. Med. Chem.* **2005**, *48*, 1630.
(38) Park, H.; Brothers, E. N.; Merz, K. M., Jr. *J. Am. Chem. Soc.* **2005**, *127*, 4232.
(39) Xu, D.; Zhou, Y.; Xie, D.; Guo, H. *J. Med. Chem.* **2005**, *48*, 6679.
(40) Estiu, G.; Suarez, D.; Merz, K. M., Jr. *J. Comput. Chem.* **2006**, *27*, 1240.
(41) Dal Peraro, M.; Llarrull, L. I.; Rothlisberger, U.; Vila, A. J.; Carloni, P. *J. Am. Chem. Soc.* **2004**, *126*, 12661.
(42) Xu, D.; Xie, D.; Guo, H. *J. Biol. Chem.* **2006**, *281*, 8740.
(43) Dal Peraro, M.; Vila, A. J.; Carloni, P.; Klein, M. L. *J. Am. Chem. Soc.* **2007**, *129*, 2808.
(44) Elstner, M.; Porezag, D.; Jungnickel, G.; Elsner, J.; Haugk, M.; Frauenheim, T.; Suhai, S.; Seigert, G. *Phys. Rev.* **1998**, *B58*, 7260.

which has been shown to provide very encouraging results for zinc enzymes,[31,39,42,46,47] including the L1-moxalactam complex.[22] Corrections to the semiempirical method were introduced by single-point B3LYP/MM calculations along the reaction path. In addition, we present high-level density functional theory (DFT) results based on a truncated active-site model to validate the mechanistic steps unraveled by the QM/MM simulations. Such theoretical studies are important because they bridge the gap between experimental measurements and an atomistic understanding of the enzymatic process and may help the future design of new therapeutic agents that inhibit MβLs.

2. Methods

2.1. QM/MM Simulations. The hybrid quantum mechanical/molecular mechanical (QM/MM) approach is a well established tool for studying extended systems including enzymes.[48−50] The QM/MM idea[51] is simple: treating a small reactive system with accurate quantum mechanics while approximating the surroundings with a classical force field. This is necessary because the bond-breaking and bond-forming processes cannot be easily modeled by a force field, while a full quantum treatment of the enzymatic system and solvent is formidable. The QM/MM approach is also preferred for metallo-enzymes because, in principle, it offers a reliable description of both chemical and electrostatic interactions in the ligand−metal coordination and is capable of handling complications, such as a change of the coordination number, during a reaction.

Ideally, the QM part of the calculation should be treated with ab initio methods such as the density functional theory (DFT) method. However, the numerical costs of the ab initio QM/MM approach restricted its application to systems involving small QM regions.[50] For dinuclear β-lactamases such as L1, it is essential to include not only the metal ions and substrate but also the protein ligands. The large number of atoms in our system thus makes such an approach very expensive, especially for optimization and dynamics.[40] Instead, we largely relied on a recently developed approximate density functional method, namely the self-consistent charge-density functional tight binding (SCC-DFTB) method,[44] in our treatment of the QM region. The semiempirical SCC-DFTB method is based on a second-order expansion of the total DFT energy with respect to the charge-density variation. Its major advantage is its efficiency, with a speed comparable to that of other semiempirical methods such as AM1 and PM3, while offering reasonable accuracy.[45,52−55] A particularly important advance related to this work is the recent parametrization of the biological zinc, which yielded results such as geometry and ligand binding energies that are in much better agreement with the B3LYP/6-311+G** model than other semiempirical methods.[46] Recent applications of SCC-DFTB/MM to zinc enzymes have shown very encouraging results.[22,31,39,42,47] To correct the possible inaccuracies in the semiempirical SCC-DFTB method, we further carried out single-point B3LYP/MM calculations along the reaction path determined by the SCC-DFTB/MM protocol.

Following our recent work,[22] the QM region in our simulations includes the two zinc ions, the putative hydroxide ion nucleophile bridging the two metal ions, the side chains of the protein ligands (His116, His118, His196, Asp120, His121, and His263), and the entire substrate. The CHARMM van der Waals parameters were used for the 125 QM atoms. The MM region in our model was described by the CHARMM all atom force field.[56] The interface between the QM and MM regions was approximated using link atoms,[57] which were added to C_β atoms of the six protein residues. Throughout the simulations, the group-based switching approach[58] was applied to treat the nonbonded interactions, which has been shown to be essential for the L1−moxalactam complex.[22] All QM/MM calculations reported here were carried out using CHARMM[59] with either a SCC-DFTB interface[45] or a GAMESS interface.[60]

As detailed in our recent work,[22] the model ES complex was constructed from the X-ray structure of the L1 enzyme complexed with hydrolyzed moxalactam (PDB code 2AIO).[10] This is a unique feature because the mode of substrate binding was established on the basis of an experimental observation rather than on computational docking procedures as in many previous studies, which are often unreliable when metal ions are involved. The ionization states of all titratable side chains were carefully assigned, and the disulfur bond between Cys218 and Cys246 was enforced. The complex was solvated with a pre-equilibrated sphere of TIP3P waters[61] with a 25 Å radius centered at the hydroxide oxygen atom, followed by 30 ps solvent molecular dynamics (MD) with all protein and substrate molecules fixed. This process was repeated several times with randomly rotated water spheres to ensure even solvation. Stochastic boundary conditions[62] were then applied to the enzyme−substrate complex. In particular, atoms which are 25 Å away from the zinc-bridging hydroxide ion were removed, while those in the buffer zone ($22 < r < 25$ Å) were subjected to Langevin dynamics with frictions and random forces to simulate the influence of the bulk that was not included in the simulation. The atoms in the reaction zone ($r < 22$ Å) were described by Newtonian dynamics on the hybrid QM/MM potential.

To study the initial ring-opening step, we concentrated on two putative reaction coordinates. The first is associated with the nucleophilic addition (NA) of the hydroxide nucleophile to the lactam carbonyl carbon (C_8) and the associated elimination (E) of the leaving group: $d_1 = R_{O_w-C_8} - R_{C_8-N_5}$, while the second is related to the proton transfer (PT) from the nucleophilic hydroxide to $O_{\delta 1}$ of Asp120: $d_2 = R_{O_w-H_w} - R_{H_w-O_{\delta 1}}$. Our selections were based on examination of how various bonds participate during the reaction process. To understand the landscape of the reaction path, we first computed (using adiabatic mapping) the two-dimensional minimal energy surface in the aforementioned putative reaction coordinates.

To further include the fluctuation of the solvated protein, we have computed the potentials of mean force (PMFs) in both coordinates, using the SCC-DFTB/MM protocol. The minimal energy configurations along the reaction path were used as the initial structures in the PMF calculations. In the PMF calculations, umbrella sampling[63] with harmonic constraints in the 100−150 kcal/mol·Å^2 range was used in the sampling windows. A 30 ps equilibrium MD simulation was carried out to increase the temperature to 300 K and was followed by 30 ps data collection for each sampling window. Finally, the weighted histogram analysis method (WHAM)[64] was used to obtain the PMF. In the MD simulations, the SHAKE method[65] was applied to maintain all covalent bond-involved hydrogen atoms except the ones involved

(45) Cui, Q.; Elstner, M.; Kaxiras, E.; Frauenheim, T.; Karplus, M. *J. Phys. Chem. B* **2001**, *105*, 569.
(46) Elstner, M.; Cui, Q.; Munih, P.; Kaxiras, E.; Frauenheim, T.; Karplus, M. *J. Comput. Chem.* **2003**, *24*, 565.
(47) Riccardi, D.; Schaefer, P.; Yang, Y.; Yu, H.; Ghosh, N.; Prat-Resina, X.; Konig, P.; Li, G.; Xu, D.; Guo, H.; Elstener, M.; Cui, Q. *J. Phys. Chem. B* **2006**, *110*, 6458.
(48) Gao, J. *Acc. Chem. Res.* **1996**, *29*, 298.
(49) Monard, G.; Merz, K. M., Jr. *Acc. Chem. Res.* **1999**, *32*, 904.
(50) Friesner, R. A.; Guallar, V. *Annu. Rev. Phys. Chem.* **2005**, *56*, 389.
(51) Warshel, A.; Levitt, M. *J. Mol. Biol.* **1976**, *103*, 227.
(52) Kruger, T.; Elstner, M.; Schiffels, P.; Frauenheim, T. *J. Chem. Phys.* **2005**, *122*, 114110.
(53) Sattelmeyer, K. W.; Tirado-Rives, J.; Jorgensen, W. L. *J. Phys. Chem. A* **2006**, *110*, 13551.
(54) Otte, N.; Scholten, M.; Thiel, W. *J. Phys. Chem. A* **2007**, *111*, 5751.
(55) Seabra, G. d. M.; Walker, R. C.; Elstner, M.; Case, D. A.; Roitberg, A. E. *J. Phys. Chem. A* **2007**, *111*, 5655.
(56) MacKerell, A. D., Jr.; et al. *J. Phys. Chem. B* **1998**, *102*, 3586.
(57) Field, M. J.; Bash, P. A.; Karplus, M. *J. Comput. Chem.* **1990**, *11*, 700.
(58) Steinbach, P. J.; Brooks, B. R. *J. Comput. Chem.* **1994**, *15*, 667.
(59) Brooks, B. R.; Bruccoleri, R. E.; Olafson, B. D.; States, D. J.; Swaminathan, S.; Karplus, M. *J. Comput. Chem.* **1983**, *4*, 187.
(60) Eurenius, K. P.; Chatfield, D. C.; Brooks, B. R.; Hodoscek, M. *Int. J. Quantum Chem.* **1996**, *60*, 1189.
(61) Jorgensen, W. L.; Chandrasekhar, J.; Madura, J. D.; Impey, R. W.; Klein, M. L. *J. Chem. Phys.* **1983**, *79*, 926.
(62) Brooks, C. L., III; Brunger, A.; Karplus, M. *Biopolymers* **1985**, *24*, 843.
(63) Torrie, G. M.; Valleau, J. P. *J. Comput. Phys.* **1977**, *23*, 187.
(64) Kumar, S.; Bouzida, D.; Swendsen, R. H.; Kollman, P. A.; Rosenberg, J. M. *J. Comput. Chem.* **1992**, *13*, 1011.

in proton transfer, and the integration time step was 1.0 fs. Finally, the PMFs were corrected by including the difference between the SCC-DFTB/MM energy profile along the reaction path and the B3LYP/MM single-point energies along the same reaction path.

2.2. Truncated Active-Site Model and DFT. To provide an independent check on the QM/MM models described above, we have also studied the catalysis with a truncated active-site model using DFT. Such a model consists of the two metal ions, the nucleophilic OH^-, and analogues for the protein ligand and the substrate. In particular, the histidine side chain was approximated by methyl imidazole, and the aspartate side chain, by acetate. For the substrate molecule, the 7α-[(4-hydroxyphenyl)malonyl]amino group was removed, and the 1-methyltetrazolyl-5-thiolate group was replaced with a methyl group. The total number of atoms is 96. The initial guess of the ground-state complex was obtained from the optimized QM/MM structure.

The Becke3−Lee−Yang−Parr (B3LYP) exchange-correlation functional[66,67] and a standard basis set (6-31G(d)) were used in the full geometry optimization carried out to locate stationary points along the reaction path. These stationary points were connected via intrinsic reaction paths[68] and were confirmed by harmonic frequency calculations. Single-point calculations were then performed for these stationary points with a larger basis set (6-31++G(d,p)). The polarized continuum model (PCM)[69] was used to account for long-range solvent effects both in the protein environment ($\epsilon = 5$) and in water ($\epsilon = 80$). All DFT calculations were performed using Gaussian 03.[70]

3. Results

3.1. ES Complex. The structure of the ES complex optimized by the SCC-DFTB/MM protocol is illustrated in Figure 1, and some key geometric parameters are listed in Table 1. The two zinc ions are ligated by six protein ligands as well as the bridging hydroxide, and their internuclear distance of 3.55 Å is close to the experimental value of 3.68 Å.[10] The slightly shorter distance between the oxygen (O_w) moiety of the bridging ligand and Zn_1 observed in the X-ray study[10] was reproduced by our model. As shown in Table 1, the overall geometry of the metal centers predicted by our simulation is quite similar to that of the X-ray structure, which underlines the reliability of the SCC-DFTB approach in describing molecular geometry.

The ES complex features a direct substrate−metal contact. In particular, the C_4 carboxylate of the substrate displaces the "apical" water observed in the apo enzyme[9] to become the fourth ligand of Zn_2. The corresponding bond length of 2.26 Å is close to the experimental value of 2.30 Å.[10] Such a direct substrate−metal contact has also been seen experimentally in CphA from *A. hydrophila* where the sole zinc ion is in the Zn_2 position.[21] Because the C_4 carboxylate is conserved in all β-lactam antibiotics, its coordination with the Zn_2 ion is thought to represent the common mode of substrate binding in Mβ Ls.[6] In addition to the strong interaction with Zn_2, the carboxylate is also hydrogen bonded with the side chains of Ser221 and Ser223 (not shown in the figure), as evidenced by the hydrogen bond distances of 1.65 and 1.62 Å, respectively. As pointed out by Spencer et al.,[10] these serine residues are the equivalent of the conserved lysine residue in class B1 and B2 Mβ Ls, and might play an important role in substrate binding. Throughout the reaction, the strong interactions between the C_4 carboxylate and Zn_2/Ser221/Ser223 are maintained, as shown by the corresponding bond lengths listed in Table 1.

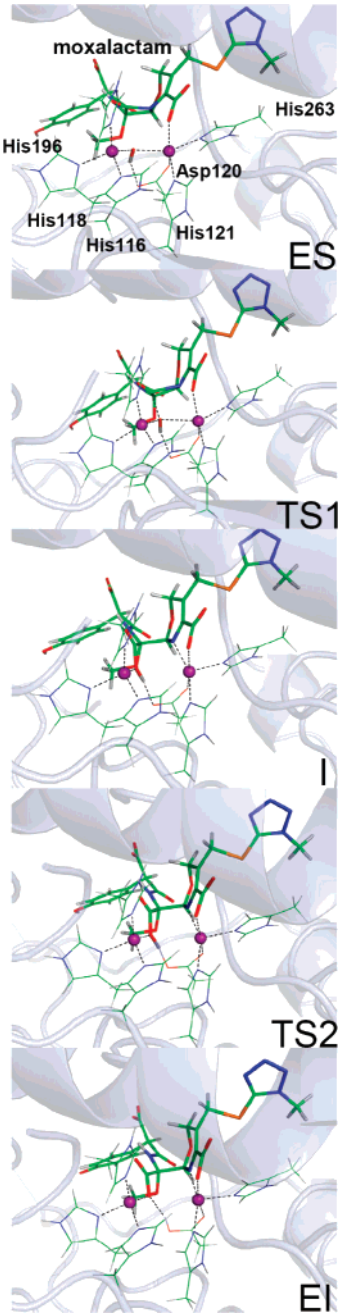

Figure 1. Snapshots of the QM/MM stationary points along the reaction path for the L1-catalyzed moxalactam hydrolysis.

Thanks to the anchoring of the C_4 carboxylate in the enzyme active site, the substrate is positioned in an ideal near-attack configuration. The distance between the nucleophilic hydroxide oxygen (O_w) and the lactam carbonyl carbon (C_8) is only 2.76 Å. In addition, the nucleophilic hydroxide bridging the two metal ions is oriented by a hydrogen bond with the nonmetal-binding $O_{\delta 1}$ of Asp120, as suggested by the X-ray data.[9,10] The carbonyl oxygen (O_9) and nitrogen (N_5) are quite close (see Table 1) to the two zinc ions, ready to tap into the positive charges provided by these electrophilic agents.

As shown in our recent study on substrate binding,[22] the aforementioned active-site structure is well maintained at room

(65) Ryckaert, J. P.; Ciccotti, G.; Berendsen, H. J. *J. Comput. Phys.* **1977**, *23*, 327.
(66) Becke, A. D. *J. Chem. Phys.* **1993**, *98*, 5648.
(67) Lee, C.; Yang, W.; Parr, R. G. *Phys. Rev. B* **1988**, *37*, 785.
(68) Gonzalez, C.; Schlegel, H. B. *J. Phys. Chem.* **1990**, *94*, 5523.
(69) Tomasi, J.; Persico, M. *Chem. Rev.* **1994**, *94*, 2027.
(70) Frisch, M. J.; et al. Gaussian, Inc.: Pittsburgh, PA, 2003.

Table 1. Selected Geometry Parameters for Stationary Points along the Reaction Path of the L1-Catalyzed Hydrolysis of Moxalactam[a]

Bond Distances (Å)

	DFT/truncated active-site model					QM/MM model					
	ES	TS1	TI	TS2	EI	ES	TS1	I	TS2	EI	expt[10]
$O_w\cdots C_8$	5.70	1.84	1.39	1.34	1.25	2.76	2.06	1.45	1.44	1.36	–
$C_8\cdots N_5$	1.38	1.42	1.63	1.99	2.86	1.42	1.85	2.18	2.20	2.52	2.75
$O_9\cdots C_8$	1.21	1.27	1.33	1.29	1.29	1.21	1.18	1.21	1.22	1.23	–
$H_w\cdot\cdot O_w$	0.99	1.01	1.01	1.03	1.63	0.99	1.00	1.04	1.10	1.98	–
$N_5\cdots Zn2$	4.84	2.77	2.15	2.05	1.93	2.99	2.88	2.08	2.08	1.98	2.38
$O_{11}\cdots Zn2$	2.20	2.09	2.07	2.18	2.06	2.26	2.20	2.25	2.23	2.15	2.30
$O_9\cdots Zn1$	5.00	2.16	1.93	1.94	1.93	3.35	3.14	2.91	2.89	2.89	
$O_w\cdots Zn1$	1.90	2.06	2.71	2.89	3.15	1.95	2.00	2.07	2.09	2.05	1.98
$O_w\cdots Zn2$	1.96	2.07	2.98	3.21	3.84	2.09	2.36	2.99	2.97	2.92	2.15
$O_{11}\cdots H_\gamma$(S221)	–	–	–	–	–	1.65	1.64	1.60	1.60	1.57	2.69[b]
$O_{12}\cdots H_\gamma$(S223)	–	–	–	–	–	1.62	1.62	1.63	1.63	1.65	2.66[b]
$Zn_1\cdots N_\delta$(H118)	2.03	2.06	2.07	2.05	2.05	2.02	2.02	2.01	2.01	2.03	2.08
$Zn_1\cdots N_\epsilon$H116)	2.02	2.08	2.03	2.05	2.05	2.05	2.04	2.01	2.01	2.04	2.20
$Zn_1\cdots N_\epsilon$(H196)	2.03	2.08	2.02	2.01	2.02	2.00	2.01	1.97	1.99	1.99	2.07
$Zn_2\cdots O_{\delta2}$(D120)	2.18	2.12	2.05	2.08	2.51	2.19	2.14	2.16	2.18	2.43	2.19
$Zn_2\cdots N_\epsilon$(H121)	2.05	2.09	2.09	2.09	2.05	2.05	2.01	2.07	2.08	2.04	2.08
$Zn_2\cdots N_\epsilon$(H263)	2.07	2.09	2.08	2.08	2.05	2.08	2.07	2.03	2.04	2.08	2.10
$H_w\cdots O_{\delta1}$(D120)	1.67	1.68	1.65	1.54	1.01	1.85	1.88	1.72	1.50	1.01	–
Zn_1-Zn_2	3.73	3.81	5.21	5.39	5.78	3.55	3.60	4.01	3.97	3.99	3.68

Angles (deg)

	DFT/truncated active-site model					QM/MM model					
	ES	TS1	TI	TS2	EI	ES	TS1	I	TS2	EI	expt[10]
$Zn_1\cdots O_w\cdots Zn_2$	150.3	–	–	–	–	122.6	–	–	–	–	125.1
$O_w\cdots Zn_1\cdots N_\epsilon$(H116)	110.5	–	–	–	–	115.3	–	–	–	–	97.2
$O_w\cdots Zn_1\cdots N_\delta$(H118)	107.2	–	–	–	–	117.2	–	–	–	–	111.6
$O_w\cdots Zn_1\cdots N_\epsilon$(H196)	108.5	–	–	–	–	121.4	–	–	–	–	135.9
$O_w\cdots Zn_2\cdots O_{11}$	94.1	–	–	–	–	88.5	–	–	–	–	91.3
$O_w\cdots Zn_2\cdots N_\epsilon$(H263)	129.0	–	–	–	–	148.5	–	–	–	–	166.4
$O_w\cdots Zn_2\cdots N_\epsilon$(H121)	116.2	–	–	–	–	100.8	–	–	–	–	97.2
$O_w\cdots Zn_2\cdots O_{\delta2}$(D120)	90.3	–	–	–	–	89.7	–	–	–	–	84.5
$O_w\cdots H_w\cdots O_{\delta1}$(D120)	171.5	–	–	–	–	152.1	–	–	–	–	–
N_ϵ(H263)$\cdots Zn_2\cdots N_\epsilon$(H121)	114.6	106.4	112.5	112.1	107.2	110.7	112.7	108.6	108.2	105.3	96.3
N_ϵ(H263)$\cdots Zn_2\cdots O_{\delta2}$(D120)	85.8	85.6	88.1	87.6	85.1	82.2	83.0	87.1	86.4	80.4	93.2
N_ϵ(H121) $\cdots Zn_2\cdots O_{\delta2}$(D120)	90.4	90.4	97.5	94.8	84.5	101.3	101.4	97.3	95.7	92.9	92.7
N_δ(H118)$\cdots Zn_1\cdots N_\epsilon$(H116)	113.2	112.2	107.8	110.2	106.5	95.0	95.5	97.8	98.2	96.4	99.4
N_δ(H118)$\cdots Zn_1\cdots N_\epsilon$(H196)	106.2	106.6	106.2	107.3	111.9	109.9	110.5	113.1	112.0	111.8	107.9
N_ϵ(H116)$\cdots Zn_1\cdots N_\epsilon$(H196)	111.0	93.7	114.9	117.1	117.0	92.2	91.7	93.5	93.3	92.3	94.9

[a]The QM/MM and DFT/truncated active-site results are also compared with available experimental data. [b] O−O distances.

temperature, although the internuclear distances are usually larger than the minimal energy configuration discussed above and in better agreement with the experimental data.

Reaction Path. The nucleophilic attack of the lactam carbonyl carbon (C_8) by the bridging hydroxide (O_w) sets off a cascade of geometric changes, culminating with an enzyme-intermediate (EI) complex featuring a cleaved lactam amide C_8-N_5 bond. Two transition states between the ES and EI complexes were found in our SCC-DFTB/MM simulations, and they flank a metastable intermediate (I) complex. The geometries of these stationary states are displayed in Figure 1, and the important internuclear distances and angles are listed in Table 1. Note that the geometry of I is a distorted tetrahedral, with an elongated C_8-N_5 bond. Although it clearly corresponds to the tetrahedral intermediate in the DFT reaction path, as discussed below, we refrain from calling it a TI.

The dominant first transition state (TS1) involves largely the shortening of the O_w-C_8 distance, which changes from 2.76 Å in ES to 2.06 Å in TS1. On the other hand, the second transition state (TS2) stems largely from the cleavage of the bond to the nitrogen leaving group, as evidenced by the elongation of the C_8-N_5 distance from 2.20 Å in TS2 to 2.52 Å in EI. Interestingly, the elimination of the leaving group is accompanied by transfer of the hydroxide proton to $O_{\delta1}$ of Asp120. To illustrate the timing of the proton-transfer relative to the nucleophilic substitution process, we display in Figure 2 a two-dimensional minimum energy surface in the two reaction coordinates. As shown by the figure, the first transition state clearly precedes the proton transfer, indicating that Asp120 is not a general base. On the other hand, the collapse of the intermediate is largely along the PT coordinate. As shown in Figure 2, the intermediate is only nominally stable and it can easily collapse to the EI complex. Despite the kinetic insignificance of the intermediate, however, the reaction does not proceed concertedly and should still be considered as stepwise.

An interesting mechanistic issue is concerned with the interaction between the hydroxide nucleophile and Zn_2. Some believed that the O_w-Zn_2 bond is broken during the nucleophilic addition to C_8 of the substrate.[6] Our QM/MM structure of the dominant transition state (TS1) indicates that the nucleophilic O_w is much closer to Zn_1 than to Zn_2. However, the O_w-Zn_2 distance of 2.99 Å seems to suggest that there is still significant interaction. This observation highlights the importance of Zn_2 and could be important for understanding the influence of the zinc content on the catalytic efficiency in MβLs.

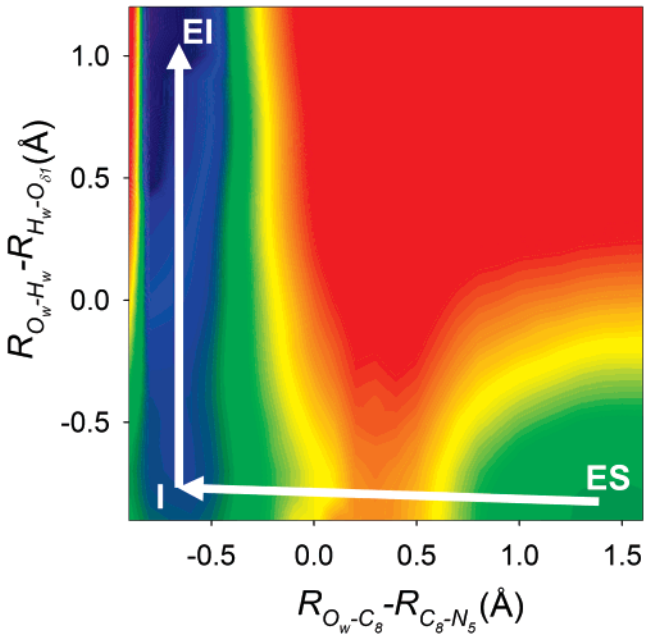

Figure 2. QM/MM minimal energy surface for the reaction and proton-transfer coordinates in the L1-catalyzed hydrolysis of moxalactam.

As shown in Figure 1, the EI complex features an opened lactam ring with a completely cleaved C_8-N_5 bond, as evidenced by the corresponding distance of 2.52 Å. The resulting leaving group nitrogen (N_5) becomes strongly ligated with Zn_2, as evidenced by the corresponding distance of 1.98 Å. In the meantime, the lactam carbonyl oxygen also forms a quite strong bond with Zn_1 ($d(O_9-Zn_1) = 2.89$ Å). The hydroxide proton is transferred to the Asp120 side chain that, as a result, weakens its coordination with Zn_2 as evidenced by the longer $O_{\delta 2}-Zn_2$ distance (2.43 Å). Although still hydrogen bonded with the transferred proton, the deprotonated O_w atom is coordinated with Zn_1, resulting in a larger Zn−Zn distance (3.99 Å).

Throughout the reaction path, the metal−ligand bonds and hydrogen bonds between the enzyme and substrate are mostly maintained. The only exception is the aforementioned Zn_2-Asp120 interaction, which is weakened because of the Asp120 protonation.

3.2. Potentials of Mean Force. Although it provides much insight into the reaction mechanism, the reaction path discussed in the previous section does not contain entropic information. To include the protein and solvent fluctuations, we have computed the PMFs along the two putative reaction coordinates, respectively. Twelve windows were used in the first segment along d_1 starting from ES to TI, while ten were used along d_2 from TI to EI.

As shown in left panel in Figure 3, the dominant first barrier has a free energy of activation of 7.9 kcal/mol, which is slightly lower than that obtained in the reaction path calculation (~11 kcal/mol). The calculated free energy barrier is significantly smaller than the experimental value (18.5 kcal/mol) derived from the turnover rate ($k_{cat} = 0.15$ s^{-1}).[20] The intermediate complex (I) was found to be unstable, but its signature is clearly discernible in the PMF. This is consistent with the reaction path results in Figure 2, where the corresponding minimum is very shallow. Finally, the ring-opening step releases 24 kcal/mol of energy, according to the free energy profile. As discussed below, the large exothermicity can be traced back to the inaccuracy of the QM model used in our simulation, which may also explain the underestimation of the rate-limiting barrier.

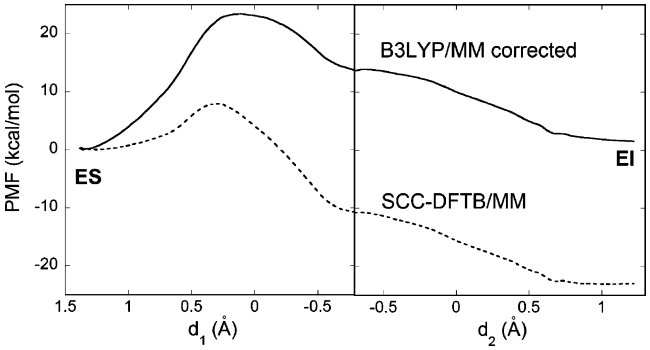

Figure 3. PMFs for the initial ring-opening step in the L1-catalyzed hydrolysis of moxalactam obtained with the SCC-DFTB/CHARMM model with (solid line) and without (dashed line) corrections based on B3LYP/MM calculations. For detail of the correction, see text.

The surprisingly large exothermicity and relatively low barrier height at TS1 in the SCC-DFTB/MM PMFs are likely due to the inherent errors in the semiempirical SCC-DFTB treatment of the QM region. Recent studies have indeed shown that SCC-DFTB tends to yield larger bonding energies than ab initio or DFT methods,[54] which might be responsible for the underestimation of barrier heights. To gauge the extent of inaccuracies, we have performed single-point B3LYP/MM calculations along the reaction path determined by the SCC-DFTB/MM protocol. As shown in Figure 2, the reaction path follows d_1 and then d_2. As a result, we have represented the reaction path in two segments, each with one reaction coordinate fixed. Since the entire substrate is included in the QM region, the number of electrons is significantly larger than that in the truncated active-site model. We have used the LANL2DZ basis set for the zinc and sulfur atoms with the effective core potentials (ECPs),[71,72] and the standard 6-31G(d) basis set for other atoms (C, O, N, and H). The B3LYP/MM energies were obtained using a GAMESS-CHARMM interface, and their differences from the corresponding SCC-DFTB/MM energies were fitted to third-order polynomials in the two reaction coordinates (d_1 and d_2), as discussed in Supporting Information. These correction terms were then added to the PMFs obtained from the SCC-DFTB/MM simulations.

The corrected PMFs, which are displayed in solid lines in Figure 3, show a much higher barrier for the nucleophilic addition without qualitatively changing the free energy profile. The free energy barrier is estimated at 23.5 kcal/mol, which represents a much better agreement with the experimental value of 18.5 kcal/mol than the original SCC-DFTB/MM value (7.9 kcal/mol). It is also in line with the barrier height (22.6 kcal/mol) determined by the truncated active-site model discussed below. In addition, the corrected PMFs indicate that the EI complex is nearly thermally neutral with the ES complex. This example highlights the limitations of semiempirical methods in studying chemical reactions and emphasizes the necessity of validation with high-level quantum chemical methods. Nonetheless, the corrections were quantitative in nature and do not change our conclusions concerning the mechanism of the reaction.

(71) Hay, P. J.; Wadt, W. R. *J. Chem. Phys.* **1985**, *82*, 270.
(72) Wadt, W. R.; Hay, P. J. *J. Chem. Phys.* **1985**, *82*, 284.

Table 2. Energetics of the Truncated Active-Site Model for L1-Catalyzed Moxalactam Hydrolysis Calculated by DFT (energy given in kcal/mol)

stationary points	ES	TS1	TI	TS2	EI
energy (B3LYP/6-31G(d))	0.00	26.9	13.3	15.2	0.3
energy (B3LYP/6-31++G(d,p)// B3LYP/6-31G(d))	0.00	28.6	14.9	16.3	0.6
free energy (B3LYP/6-31G(d))	0.00	27.0	13.1	15.0	−2.0
PCM (B3LYP/6-31G(d) w/$\epsilon = 5$)	0.00	25.05	11.55	12.43	−5.01
PCM (B3LYP/6-31G(d) w/$\epsilon = 80$)	0.00	22.6	9.0	6.8	−10.6

3.3. DFT Results for Truncated Active-Site Model. The DFT investigation of the reaction pathway in the truncated active-site model also identified five stationary points, whose energies are listed in Table 2, and their geometries are displayed in Figure 4. Since the inclusion of diffuse functions and polarization functions does not qualitatively change the energies, we used the B3LYP/6-31G(d) results in the PCM calculations.

The overall mechanism is almost identical to the QM/MM findings, with only minor differences. Specifically, the reaction path is dominated by TS1, with a barrier height of 27.0 kcal/mol, which decreases to 25.05 kcal/mol in protein ($\epsilon = 5$) and 22.6 kcal/mol in water ($\epsilon = 80$). We stress that the truncated active-site model is used here to examine the qualitative aspects of the reaction. Because of the lack of a protein environment surrounding the active site, such a model cannot be expected to generate quantitatively accurate results.

The TI features a sp^3 hybridized C_8 and is metastable with a small (1.9 kcal/mol) barrier toward EI. When solvent effects are included, this intermediate becomes either less stable ($\epsilon = 5$) or even unstable ($\epsilon = 80$). It is important to note that PT from the hydroxide to Asp120 $O_{\delta 1}$ is also associated with the second transition state, in complete agreement with the reaction path obtained with the SCC-DFTB/MM model. In addition, the partial reaction is nearly thermal neutral in the gas phase, but the exothermicity increases to ∼5 kcal/mol in protein or ∼10 kcal/mol in water.

As shown in Table 1, the geometries of the ES and EI complexes are similar to those obtained in the SCC-DFTB/MM simulation. Some nonbonded distances, such as $d(O_w-C_8)$ in ES and $d(C_8-N_5)$ in EI, are larger in the truncated active-site model. The deviations from the QM/MM structures are understandable since the active-site model lacks geometric constraints imposed by the relatively rigid protein backbone. As a result, the QM/MM geometry is probably closer to reality. Similarly, the large Zn_1-Zn_2 distance in EI should not be taken seriously for the same reason. On the other hand, the internuclear distances in both transition states and in the TI are qualitatively similar to the QM/MM results, although TS1 in the QM/MM seems to be less advanced in the nucleophilic addition coordinate (O_w-C_8) and more so in the elimination coordinate (C_8-N_5). The final EI complex also features direct N_5 ligation with Zn_2 and the weakening of the interaction between Zn_2 and Asp120. The most conspicuous difference between the truncated active-site and QM/MM models is the interaction of the Zn_1 ion with the newly formed C_8 carboxylate. The DFT results clearly indicate a strong interaction between Zn_1 and the lactam carbonyl oxygen (O_9), implicating the metal ion as an oxyanion hole, while the QM/MM simulation shows a strong Zn_1-O_w interaction. Although the two oxygen atoms are equivalent in the EI complex, their mechanistic roles are different.

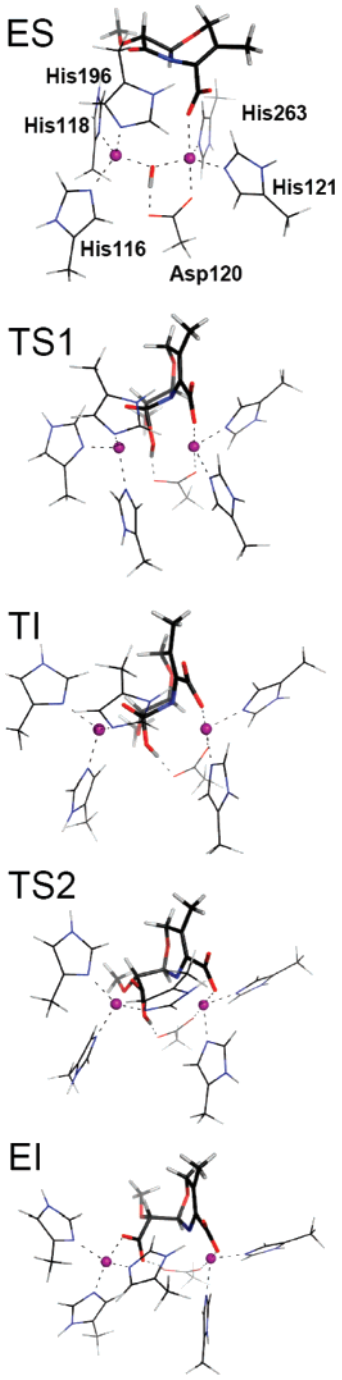

Figure 4. Stationary points along the reaction pathway of the L1-catalyzed hydrolysis of moxalactam at the B3LYP/6-31G* level of theory.

Throughout the reaction, both zinc ions are tightly ligated by the protein ligands, with the only exception of Asp120 which is protonated in EI. The increasingly larger Zn−Zn distance along the reaction path is again due to the lack of structural restraints absent in the truncated active-site model.

4. Discussion

Both the QM/MM and DFT results call for a stepwise mechanism in the initial lactam ring-opening reaction catalyzed by L1. However, the intermediate flanked by TS1 and TS2 is only nominally stable and probably kinetically insignificant. This picture is consistent with the existing mechanism proposed earlier[6,23] but provides much more detail, as shown in Scheme

1. Specifically, the reaction is initiated by the zinc-bridging hydroxide attacking the lactam carbonyl carbon, which are well aligned in the enzyme−substrate (ES) complex. The corresponding nucleophilic addition barrier is rate-limiting in the ring-opening partial reaction, and it does not require Asp120 as the general base. The resulting metastable intermediate is very unstable and readily dissociates toward the enzyme−intermediate (EI) complex. This elimination barrier is not only responsible for the eventual cleavage of the amide bond but also involves the transfer of the hydroxide proton to Asp120. The product of this partial reaction, namely the EI complex, features a direct ligation of the nitrogen leaving group with Zn_2, and of the C_8 carboxylate with Zn_1. The subsequent steps of the hydrolysis, which are not considered here, possibly include substrate rearrangements, protonation of the nitrogen to yield the final product, and the repopulation of the bridge site by a hydroxide molecule. According to Spencer et al.,[13] however, the rate of the hydrolysis reaction for most β-lactam compounds is limited by the ring-opening partial reaction.

An important difference of the current theoretical study from previous ones is the unambiguous mode of substrate binding[22] established on the basis of the latest X-ray structure.[10] The anchoring points for the binding of bicyclic penicillin compounds include the direct ligation of the C_3/C_4 carboxylate to Zn_2, and its hydrogen bonds with Ser221/Ser223 (or their equivalent Lys residue),[10] although mutagenesis data indicated that the latter is less important.[14] This binding mode makes possible two important events, namely the optimal near-attack configuration between the lactam ring and the zinc-bridging hydroxide nucleophile, and the stabilization of the nitrogen leaving group by the Zn_2 ion. It is interesting to note that the substrate binding mode in this work is quite different from a recent QM/MM study of CcrA from *Bacteroides fragilis*, in which the C_3/C_4 carboxylate was assumed to interact with Zn_2 indirectly through a water molecule.[43] This assumption is highly questionable, because existing X-ray structures of dizinc β-lactamases complexed with substrate analogues all point to direct coordination of Zn_2 by the C_3/C_4 carboxylate.[10,21,73] These structural data were also supported by theoretical studies.[22,39] In addition, the mechanism proposed by Dal Peraro et al.[43] does not include the direct coordination of the nitrogen leaving group with Zn_2 and is thus in conflict with the well-established experimental evidence in support of such a complex.[18,24−26] These differences highlight the need to establish the unambiguous mode of substrate binding in order to understand the catalytic mechanism.

An important pillar of the near-attack configuration in the dizinc Mβ*L* active site is the hydrogen bond between the hydroxide nucleophile and the side chain of the highly conserved metal-bound Asp120. This hydrogen bond, which was shown to be quite stable in several MD studies,[22,29,30,37,38] clearly plays a role in orienting the nucleophile for attacking the substrate lactam ring. Site-directed mutagenesis experiments also have shown its pivotal role in metal binding and in catalysis.[16,74] In particular, the D120N mutant of L1, which is capable of providing a weaker hydrogen bond acceptor though the $-NH_2$ group, was shown experimentally to be more viable than the D120C mutant, which has no hydrogen bond acceptor.[16]

In our earlier work on CphA hydrolysis of biapenam, the metal-bound Asp120 was identified as the general base that activates the active-site water nucleophile.[42] The situation here is different in two aspects. First, the nucleophile in L1 is metal bound, whereas that in CphA is not. Second, the zinc-bridging hydroxide is already a good nucleophile and thus requires no activation. Hence, it is not surprising that no proton transfer was observed in association with the initial nucleophilic addition step.

The existence of a TI, albeit metastable, was a surprise, because a recent DFT study on the dizinc CcrA from *Bacteroides fragilis* indicated no such intermediate.[38] However, an important difference exists in the substrate-binding pattern: the ES complex in that study did not involve direct C_3/C_4 carboxylate coordination of Zn_2, which has recently been recognized as an important determinant for substrate binding.[6] We emphasize that the existence of the TI is conceptually important, allowing us to classify the reaction as stepwise, but it has little kinetic significance.

The ligation of Zn_2 by the N_5 in the EI complex is consistent with earlier speculation that the anionic leaving group is stabilized by the metal ion.[12,13,25,26] Indeed, a recent EPR study with a Co(II)-substituted L1 confirmed that the intermediate is metal bound.[18] In addition, a hydrolysis intermediate was found to have its N_5 ligated with the Zn ion in the monozinc CphA enzyme.[21] Furthermore, DFT and QM/MM studies have also observed such an interaction in two different Mβ*L*s.[38,42] This evidence strongly suggests an important role for Zn_2 in both substrate binding and catalysis. The latter is realized by providing stabilization to the nitrogen leaving group, as initially suggested by Wang et al.[23,25]

Because of the new N_5-Zn_2 bond and the weakened $O_{\delta 2}-Zn_2$ interaction in the EI complex, the coordination sphere of Zn_2 is somewhat distorted from the canonical tetrahedral shape. This is consistent with the observed change in the EPR signal that suggests a higher coordination number of Co(II) in the intermediate.[18] However, the structural data are inconclusive for a clear transition of the metal coordination sphere. To obtain more specifics on the nature of these ligands, higher resolution studies are certainly needed.

In contrast to Zn_2, the role of Zn_1 in the catalysis is still not quite clear. Our earlier MD study of the ES complex did not reveal a strong interaction between Zn_1 and the lactam carbonyl oxygen (O_9), and neither did the current QM/MM study of the reaction path. However, the DFT results seem to suggest that it serves as an oxyanion hole during the nucleophilic attack of the hydroxide nucleophile to the carbonyl carbon. Such an oxyanion provides stabilization to the negative charge developed on the carbonyl oxygen, thus lowering the transition state. We believe that this is the likely role for the Zn_1 ion, but more studies are needed to confirm this point. On the other hand, both the QM/MM and truncated active-site models indicate that Zn_1 is important in binding the hydrolyzed substrate through direct coordination via the newly formed C_8 carboxylate.

5. Conclusions

Despite their apparent importance, theoretical studies of Mβ*L* catalysis, particularly for those with two zinc cofactors, are quite

(73) Toney, J. H.; Hammond, G. G.; Fitzgerald, P. M.; Sharma, N.; Balkovec, J. M.; Rouen, G. P.; Olson, S. H.; Hammond, M. L.; Greenlee, M. L.; Gao, Y.-D. *J. Biol. Chem.* **2001**, *276*, 31913.
(74) Yamaguchi, Y.; Kuroki, T.; Yasuzawa, H.; Higashi, T.; Jin, W.; Kawanami, A.; Yamagata, Y.; Arakawa, Y.; Goto, M.; Kurosaki, H. *J. Biol. Chem.* **2005**, *280*, 20824.

scarce. The difficulties stem mainly from the fact that a large portion of the enzyme active site and the transition metal ions have to be described quantum mechanically. In this work, we report a detailed QM/MM study of the catalysis of a dizinc β-lactamase, namely the hydrolysis of moxalactam by L1 from *S. maltophilia*. Both the reaction path and potentials of mean force have been calculated, and they revealed intimate details of the enzymatic reaction. This was made possible by an efficient semiempirical density functional method, namely SCC-DFTB, coupled with the classical CHARMM force field. Comparison with both experimental data and high level DFT results indicated that SCC-DFTB is capable of generating accurate molecular geometry and qualitatively correct reaction profiles.

We have discussed in this work two theoretical models aimed at understanding the catalysis of MβLs. Both the SCC-DFTB/MM and DFT/truncated active-site model are in qualitative agreement concerning the mechanism of the initial ring-opening partial reaction catalyzed by L1. In addition, the B3LYP/MM-corrected PMFs are in reasonable agreement with both the experimental findings and the results of the truncated active-site model. To summarize, this reaction is dominated by a nucleophilic addition barrier, while the resulting intermediate complex is unstable and readily decays to an intermediate by bond cleavage to the leaving group, concerted with proton transfer to the metal-binding Asp120. One of the zinc ions (Zn_2) provides stabilization to the anionic nitrogen leaving group, while the other (Zn_1) stabilizes the newly formed carboxylate in the C_8 position. The current theoretical study provides strong evidence in support of the proposed mechanism. Subsequent steps, which are not studied in the present work, would have to include the protonation of the nitrogen group and the replenishment of the bridging hydroxide. The reaction pathways for these processes are much less defined and require further investigations.

Acknowledgment. This work was supported by National Institutes of Health (R03AI068672) and National Science Foundation (MCB-0313743). Q.C. acknowledges National Science Foundation (CHE-0348649). Some of the calculations were carried out at the National Centers for Supercomputing Applications (NCSA).

Supporting Information Available: Details of the energy correction to the SCC-DFTB/MM reaction paths, the Cartesian coordinates of all stationary point structures calculated at the B3LYP/6-31G(d) level of theory, and full citations of refs 56 and 70. This material is available free of charge via the Internet at http://pubs.acs.org.

JA072532M